Journal of Science and Technology – Engineering and Technology for Sustainable Development
Volume 36, Issue 4, October 2026, 001–008

Synthesis and Characterization of Regenerated Cellulose Composite Membranes for Sustainable Photocatalytic Wastewater Treatment

Nguyen Quynh Vi, Truong Minh Thu, Nguyen Ngoc Mai*
Hanoi University of Science and Technology, Ha Noi, Vietnam
**Corresponding author email:* mai.nguyenngoc@hust.edu.vn

Abstract

The study investigates the influence of various photocatalysts, when incorporated into Regenerated Cellulose composite Membranes (RCMs), on the resulting structural properties and photocatalytic degradation performance. Three distinct composite membranes (RCMP25, RCMP25Cu, and RCMP25Ce) were successfully synthesized via a process involving dissolution of cellulose and subsequent coagulation. The successful incorporation of the catalysts and structure of membrane were confirmed by Fourier-transform infrared spectroscopy, X-ray diffraction, Inductively Coupled Plasma Optical Emission Spectroscopy, and Scanning Electron Microscopy. Notably, elemental Ti mapping further demonstrated a uniform distribution of the catalyst particles across the membrane surface. Differential Scanning Calorimetry analysis revealed that the thermal characteristics of the membranes remained essentially unchanged despite the incorporation of different catalysts. In terms of performance, the RCMP25Cu membrane exhibited significant adsorption capabilities under dark conditions, removing up to 32.3% of Rhodamine B (RhB), and achieved the highest degradation efficiency for Methylene Blue (81.91%). Conversely, the RCMP25Ce membrane displayed superior photocatalytic activity toward RhB, reaching 84.89% degradation after 120 minutes of illumination under a Xenon lamp (95% visible light). Therefore, the RCMs exhibit remarkable versatility, enabling the incorporation of diverse photocatalysts for the adsorption and degradation of cationic pollutants without altering their structural integrity, phase composition, and morphology. This research highlights the potential of sustainable cellulose-based platforms for advancing next-generation composite membranes in water treatment applications.

Keywords: Cellulose, organic dyes, photocatalyst, regenerated cellulose composite membranes, wastewater treatment.

1. Introduction

Organic dyes (ODs) contamination poses a serious and persistent threat to aquatic environments, primarily driven by the rapid growth of dye-consuming industrial sectors. Owing to their chemically stable aromatic structures, ODs are notoriously resistant to natural degradation, allowing them to linger in rivers and lakes for extended periods following industrial discharge. The presence of these pollutants in water bodies not only reduces transparency and hinders light penetration but also severely disrupts normal ecological functions [1, 2]. With industrial expansion, the demand for reliable and sustainable solutions to safeguard water quality has become increasingly urgent.

Among the various materials explored for water treatment, cellulose membranes have gained increasing attention due to their intrinsic sustainability and functional versatility. Derived from renewable biomass, cellulose exhibits biodegradability, hydrophilicity, and a dense network of hydroxyl groups that facilitate strong interactions with dissolved pollutants [3]. When processed into regenerated membranes, these features result in excellent wettability, high permeability, and dependable adsorption performance. Furthermore, the introduction of functional additives into cellulose to fabricate composite membranes offers an effective route to reinforce mechanical integrity, improve thermal stability, and enhance pollutant adsorption while allowing the separation behavior to be adjusted toward targeted contaminants [4]. As a result, the development of regenerated cellulose composite membranes has gained increasing interest as a sustainable and effective solution for modern water treatment technologies.

Photocatalysis has long been acknowledged as one of the most ecological and energy-efficient ways for reducing organic contaminants in water [5]. Photocatalysts use light, particularly visible light, as a driving force to create reactive oxygen species capable of breaking down complicated dye molecules and eventually mineralizing them into ecologically nontoxic compounds such as CO_2 and H_2O. Among various photocatalytic materials, TiO_2 (P25) and its metal-modified derivatives remain the most extensively studied due to their high oxidative potential, structural stability, low cost, and non-toxicity [6]. These qualities make them appealing options for environmentally friendly water filtration methods. However, when used in actual water treatment environments, powdered photocatalysts encounter major challenges. Because of their great dispersibility due to their nanoscale or microscale particle size, post-treatment separation is quite difficult. Without an effective recovery process, catalyst residues can stay suspended in treated water,

p-ISSN 3093-3242
e-ISSN 3093-3579
https://doi.org/10.51316/jst.192.etsd.2026.36.4.x
Received: Dec 16, 2025; Revised: Feb 1, 2026;
Accepted: Feb 4, 2026; Online: Jun 17, 2026

increasing turbidity and raising the risk of secondary contamination. Furthermore, in practical applications, the frequent loss of catalyst mass lowers photocatalytic efficiency over time, resulting in poor reusability and increased operating costs. For large-scale continuous water treatment, conventional recovery methods like centrifugation, sedimentation, or filtration are inefficient, time-consuming, and energy intensive.

To address these limitations, immobilizing photocatalysts onto solid supports has emerged as a promising strategy, among which regenerated cellulose membranes stand out as an ideal base material. The membrane matrix provides abundant surface functional groups and a porous architecture that favors strong attachment of catalyst particles. When incorporated into the cellulose structure, the photocatalyst becomes stably anchored, preventing leaching during operation while ensuring intimate contact between pollutants and active sites. In addition, cellulose inherently exhibits excellent hydrophilicity and adsorption capacity, which promotes the pre-concentration of pollutant molecules onto the membrane surface – an essential step that enhances photocatalytic efficiency [5, 7]. This synergistic combination allows adsorption and photodegradation to occur simultaneously on a single composite platform. Importantly, because the catalyst remains fixed within the membrane, the entire material can be retrieved and reused easily, eliminating the need for additional recovery steps and enabling more sustainable and practical water-treatment operations.

In this study, regenerated cellulose composite membranes (RCMs) were synthesized by immobilizing different photocatalyst powders onto the cellulose matrix. The RCMs (RCMP25, RCMP25Cu, and RCMP25Ce) were prepared using a simple process, enabling the effective incorporation of P25, P25 doped copper (P25Cu), and P25 doped cerium (P25Ce). After that, RCMs' structural properties and photocatalytic performance are evaluated and compared. Elemental compositions were quantified using inductively coupled plasma optical emission spectroscopy (ICP-OES) and the successful formation of the composites was further confirmed by Fourier-transform infrared spectroscopy (FTIR), X-ray diffraction (XRD), and X-ray photoelectron spectroscopy (XPS). Surface and cross-sectional morphologies were examined by scanning electron microscopy (SEM), while elemental Ti mapping verified the uniform distribution of catalyst particles across the membrane surface. The photocatalytic activity of the RCMs was assessed under predominantly visible-light illumination from a Xenon lamp using three representative ODs: Methylene Blue (MB), Rhodamine B (RhB), and Methyl Orange (MO). Ultraviolet–Visible Spectroscopy (UV–Vis) spectral analysis enabled quantitative tracking of dye degradation over time. The results demonstrate that the regenerated cellulose platform can effectively immobilize various photocatalysts while supporting their activity toward the degradation of cationic organic pollutants. These findings highlight the potential of cellulose-based composite membranes as adaptable and sustainable materials for next-generation water treatment technologies, with broad opportunities for future modification to target diverse contaminant classes.

2. Materials and Methods

2.1. Materials

Microcrystalline cellulose (MCC, 20 μm, powder), propylene carbonate (PC, 99.7%, solution), dimethyl sulfoxide (DMSO, 99.9%, solution), copper(II) nitrate trihydrate ($Cu(NO_3)_2.3H_2O$, powder), and cerium(III) nitrate hexahydrate ($Ce(NO_3)_3.6H_2O$, powder) were purchased from Sigma-Aldrich. Acros produced tetrabutylphosphonium hydroxide (TBPH, 40 *wt.*% solution). Methyl Orange (MO, powder), Rhodamine B (RhB, powder), and Methylene Blue (MB, powder) were obtained from Merck. Titanium dioxide (P25, powder) was provided by Evonik.

2.2. Methods

2.2.1. The preparation of regenerated cellulose composite membranes

The preparation of RCMs with different photocatalysts via the coagulation method consisted of five steps, as illustrated in Fig. 1. Initially, cellulose was dissolved with tetrabutylphosphonium hydroxide (TBPH) and dimethyl sulfoxide (DMSO) at the investigated ratio of 1:0.3 [8]. To achieve the required concentration for cellulose dissolution, the commercial TBPH 40 *wt.*% solution was concentrated to 50 *wt.*% using a rotary evaporator at 60 °C under reduced pressure [9]. Then, added 10 mg of each photocatalyst powder to the cellulose solution [7]. After that, the mixtures were stirred and poured onto the glass surface. Next, the glass was immersed in the coagulation bath to form the membrane for 30 minutes. Finally, all membranes were washed with distilled water and cut into circular shapes for further experiments, namely RCMP25, RCMP25Cu, and RCMP25Ce.

To dope other metals onto the commercial P25 catalyst via wet impregnation, pre-calculated amounts of $Cu(NO_3)_2.3H_2O$ and $Ce(NO_3)_3.6H_2O$ were dissolved in distilled water. Subsequently, P25 powder was added to the solution and stirred vigorously for 24 hours at room temperature. After washing with distilled water, the precipitates were dried at 100 °C for 24 hours and then calcined at 500 °C for 4 hours. The final photocatalysts were obtained and designated as P25Cu and P25Ce [10].

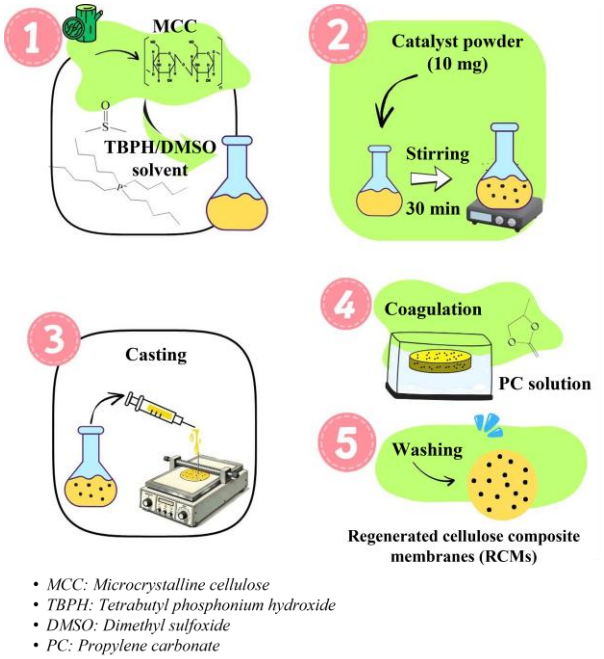

Fig. 1. Schematic overview of incorporating different photocatalysts with regenerated cellulose membrane

2.2.2. The methods of characterization

Three composite membranes (RCMP25, RCMP25Cu, and RCMP25Ce), together with a reference membrane (RCM without catalysts) were characterized using a Fourier-transform infrared spectroscopy (FTIR) spectrometer (Nicolet iS50, Thermo Fisher Scientific) operating in ATR mode over the wavenumber range of 400 – 4000 cm^{-1}.

These samples are also examined by an X-ray diffraction (XRD) employing Cu kα radiation (40 kV, 35 mA) on X'Pert Pro (PANalytical) diffractometer. Three composite membranes were mounted on a stainless-steel holder for XPS measurements, which were carried out by an ESCALAB 220iXL (Thermo Fisher Scientific) equipped with Al *Kα* radiation (*E* = 1486.6 eV).

The surface, cross-sectional, and energy-dispersive X-ray spectroscopy (EDS) of composite membranes are obtained on JEOL JCM-7000 BENCHTOP SEM. The content of Cu, Ce, and Ti in samples was determined by Inductively Coupled Plasma Optical Emission Spectroscopy (ICP/OES) with Varian/Agilent 715-ES.

Differential scanning calorimetry (DSC) of three composite membranes were subjected to a NETZSCH STA 449F5 calorimetric analyzer under an air atmosphere with a temperature range of 50 ºC to 400 ºC and a heating rate of 10 $K.min^{-1}$.

The porosity (ε) of cellulose membranes were calculated by the following equation:

$$\varepsilon\ (\%) = \frac{w-w'}{\rho.S.d}.100 \quad (1)$$

where *w* and *w'* are the wet and dry membrane weights, respectively; ρ equal 0.998 g/cm^3 is the density of water; *S* is the membrane area (cm^2); and *d* is the thickness of the membrane (cm).

2.2.3. Investigation of the photocatalytic performance

The removal efficiency (*RE*) was calculated using the following equation:

$$RE\ (\%) = \frac{C_0-C_t}{C_0}.100 \quad (2)$$

in which, C_0 is the initial concentration of pollutants (ODs) (ppm), C_t is the concentration of pollutants after *t* (minutes) of treatment. The pollutant concentration was extrapolated by the standard curve method.

The photocatalytic performance of samples was studied through the adsorption in the dark and the decomposition under Xenon illumination (5% UV, 300 W, LSE341, LOT Quantum Design, wavelength: 300–700 nm, light intensity: 1000 mW cm^{-2}). The UV-Vis analysis was used to determine the residual of MB, RhB, and MO after treatment by the catalysts. In the illumination period, the degradation of ODs in an aqueous solution follows a first-order kinetic equation described by the equation:

$$ln\left(\frac{C_0}{C_t}\right) = k_1 t \quad (3)$$

in which C_0 is the initial concentration of OD (ppm), C_t is the concentration of pollutants after the treatment; k_1 is the reaction rate constant (min^{-1}), and *t* is the time in minutes.

3. Results and Discussion

3.1. The Structure of Composite Membranes

Fig. 2a presents the FTIR spectra of the regenerated cellulose membrane (without catalyst) and the RCMs, including RCMP25, RCMP25Cu, and RCMP25Ce. It can be observed that all three composite membranes exhibit vibration bands similar to those of the pristine cellulose membrane. In particular, the broad absorption bands located at approximately 3300 cm^{-1} and 1600 cm^{-1} are attributed to O–H stretching and O–H bending vibrations, respectively. The characteristic cellulose peaks, including C–H stretching, C–H bending, and C–O–C stretching vibrations, are also clearly observed at around 2890 cm^{-1}, 1370 cm^{-1}, and 1000 cm^{-1}, respectively [11]. These results indicate that the regenerated cellulose membranes were successfully synthesized and are capable of immobilizing photocatalyst powders without altering the intrinsic chemical bonds of the cellulose matrix. To obtain a more detailed and reliable understanding of the structural and phase characteristics of the prepared RCMs, XRD analysis was further performed on the corresponding samples, as shown in Fig. 2b.

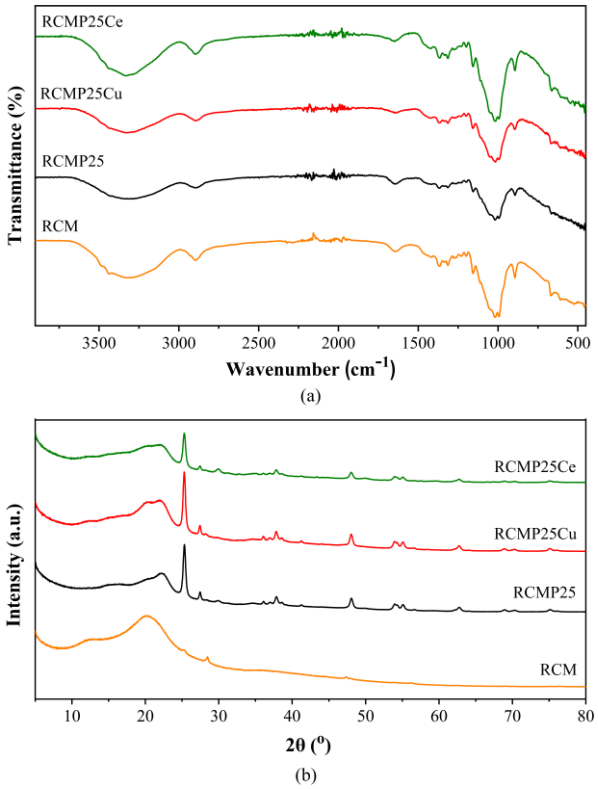

Fig. 1. (a) FTIR spectra and (b) XRD patterns of three composite membranes with reference sample – membrane without catalyst

It can be observed that both the regenerated cellulose membrane and the three catalyst-loaded composite membranes exhibit the characteristic cellulose II crystalline phase, with a dominant diffraction peak located at approximately 20°–21° and a minor peak around 12°. This observation is consistent with our previous studies, which demonstrated that the incorporation of photocatalyst particles into the cellulose matrix does not alter the crystalline phase structure of regenerated cellulose [12]. In addition, the P25 catalyst embedded within the membranes displays the coexistence of anatase and rutile phases, in good agreement with the specifications provided by Evonik. These results confirm that the interaction between the cellulose membrane and the photocatalyst particles is primarily physical in nature. The regenerated cellulose framework effectively entraps the fine catalyst particles within the membrane matrix without affecting the chemical bonding, phase composition, or crystalline structure of either the cellulose or the photocatalyst.

Since no characteristic diffraction peaks corresponding to copper- or cerium-containing species were detected in the XRD patterns of RCMP25Cu and RCMP25Ce, XPS was further employed to confirm the presence of these elements and to identify their oxidation states on the surface of the composite membranes.

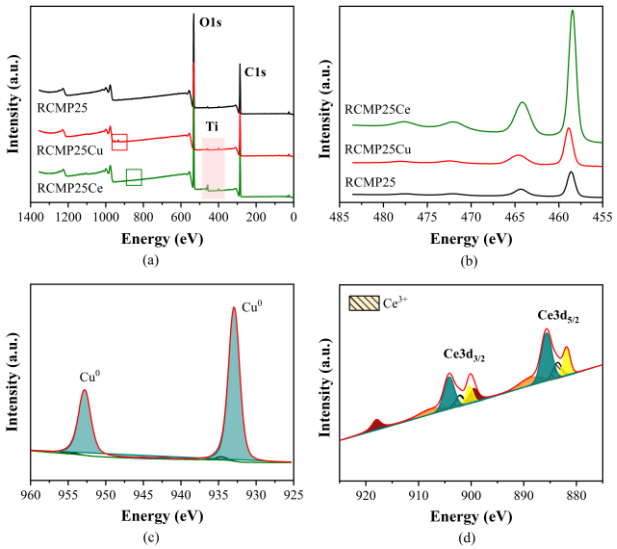

Fig. 2. (a) XPS spectra of three composite membranes and the high-resolution spectra of (b) Ti2p, (c) Cu2p, and (d) Ce3d

As illustrated in Fig. 3a, the XPS survey spectra of the three RCMs exhibit characteristic signals corresponding to carbon (284 eV), oxygen (533 eV), and titanium (458 eV). Fig. 3b presents the high-resolution Ti2p spectra, which display two distinct peaks at approximately 458 eV and 464 eV, assigned to Ti $2p_{3/2}$ and Ti $2p_{1/2}$, respectively, confirming the presence of Ti in the +4 oxidation state [13]. In addition, weak but discernible signals of copper and cerium are observed in the RCMP25Cu and RCMP25Ce samples, respectively. The high-resolution Cu2p spectrum of RCMP25Cu (Fig. 3c) shows two main peaks at around 934 eV and 953 eV, which are attributed to the Cu $2p_{3/2}$ and Cu $2p_{1/2}$ levels, indicating the presence of Cu species on the membrane surface. For the RCMP25Ce sample, the high-resolution Ce3d spectrum (Fig. 3d) reveals a series of overlapping peaks in the binding energy range of 800–910 eV, characteristic of the coexistence of Ce^{3+} (900, 902, and 905 eV) and Ce^{4+} (908 and 898 eV) oxidation states. This result is consistent with the literature review about the XPS spectra of cerium [14]. This mixed-valence nature is commonly associated with enhanced redox capability and oxygen vacancy formation in cerium-containing photocatalysts.

3.2. The Morphology and Properties of Composite Membranes

Fig. 4 presents the SEM images of the surface, cross-sectional morphology, and Ti elemental mapping of the RCMs (RCMP25, RCMP25Cu, and RCMP25Ce). It can be clearly observed that the surfaces of the composite cellulose membranes retain morphological features similar to those of regenerated cellulose membranes; however, they are no longer smooth and uniform due to the presence of finely dispersed photocatalyst particles. Cross-sectional images reveal

the characteristic layered structure of regenerated cellulose, along with the presence of small crystalline domains that are attributed to the embedded photocatalyst particles within the membrane matrix.

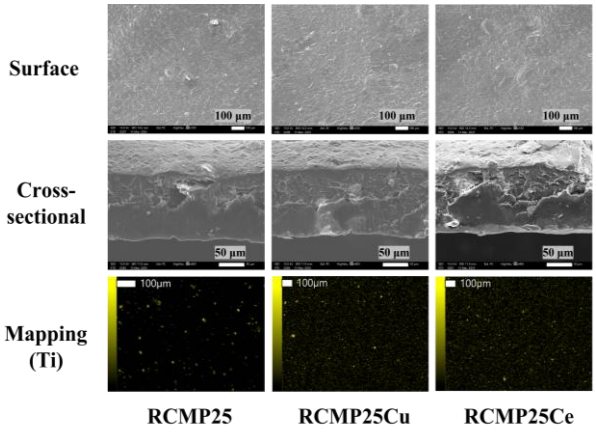

Fig. 3. SEM images of the surface and cross-section of all membranes and Ti elemental mapping

No significant differences in membrane thickness are observed among the samples containing different catalysts, and the detailed thickness values are summarized in Table 1. Furthermore, the Ti elemental mapping images confirm the successful incorporation of the photocatalysts into the membranes and demonstrate a relatively uniform distribution of Ti across the membrane surface. The corresponding metal contents of the membranes are also quantitatively reported in Table 1.

Table 1. Summary properties of three membranes

	RCMP25	RCMP25Cu	RCMP25Ce
% Metal (ICP/OES)	%Ti = 6.37	%Ti = 6.16 %Cu = 0.20	%Ti = 5.53 %Ce = 0.01
% Mass (EDS)	%Ti = 5.37	%Ti = 1.09 %Cu = 0.05	%Ti = 1.76 %Ce = 0.09
Thickness (μm)	96.1	126.1	120.3
Porosity (%)	76.47	83.64	79.70

The influence of incorporating different photocatalysts on the thermal properties of regenerated cellulose membranes was also investigated, as shown in Fig. 5. Fig. 5 presents the DSC thermograms of the RCMP25, RCMP25Cu, and RCMP25Ce membranes recorded over a temperature range of 50 °C – 400 °C. These curves display a single endothermic peak at approximately 269 °C, 275 °C, and 237 °C, respectively, which is attributed to the thermal degradation of the regenerated cellulose. The absence of additional thermal transitions confirms that the incorporation of different photocatalysts does not induce new thermal events or disrupt the intrinsic thermal behavior of cellulose. This observation is consistent with the FTIR and XRD results, which indicate that the cellulose backbone and phase structure remain unchanged after catalyst immobilization. The slight variation in peak temperature among the membranes may arise from weak physical interactions and differences in heat dissipation caused by the embedded catalyst particles. Overall, these results demonstrate that the photocatalysts are physically immobilized within the cellulose matrix without compromising its thermal stability.

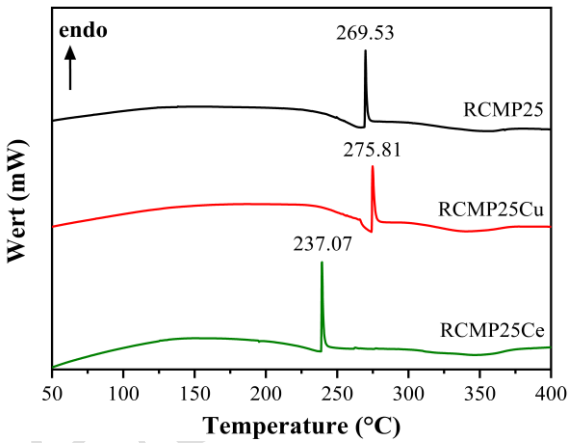

Fig. 4. DSC curves of three composite membranes in the range of 50 °C to 400 °C

3.3. Photoactivity of Composite Membranes

Fig. 6 presents the UV–Vis absorption spectra of the ODs used to evaluate the photocatalytic performance of the RCMs, namely MB, MO, and RhB. The maximum absorption wavelengths (λ_{max}) of MB, MO, and RhB are observed at 664 nm, 465 nm, and 552 nm, respectively. Accordingly, the temporal changes in absorbance at these wavelengths were monitored to quantify the dye concentration during the treatment process and to calculate the degradation efficiency of the RCMs using (2).

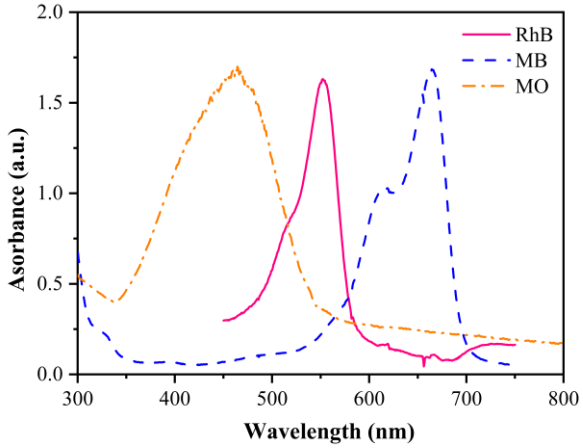

Fig. 5. UV-Vis spectra of Rhodamine B, Methylene Blue, and Methyl Orange under visible wavelengths

Before conducting the photocatalytic experiments, the adsorption capacity of the membranes for each dye was evaluated under dark conditions. Circular membranes with a diameter of 24 mm were immersed in the dye solution to assess their adsorption capacity. The adsorption results are summarized in Fig. 7 for the different membrane groups. In general, all RCMs samples reached adsorption equilibrium after approximately 50 minutes. For RCMP25, the adsorption efficiency for MO, MB, and RhB after 70 minutes was 4.4%, 12.1%, and 10.1%, respectively, indicating that the cellulose-based membrane had a higher affinity for MB and RhB than for MO. A similar trend was also observed for the RCMP25Cu and RCMP25Ce membranes. Specifically, RCMP25Cu exhibited adsorption efficiencies of 20.4% for MB and 32.3% for RhB, whereas only 4.5% of MO was adsorbed after 70 minutes. Similarly, RCMP25Ce adsorbed 21.4% of MB and 29.9% of RhB, while MO adsorption remained low at 3.9%.

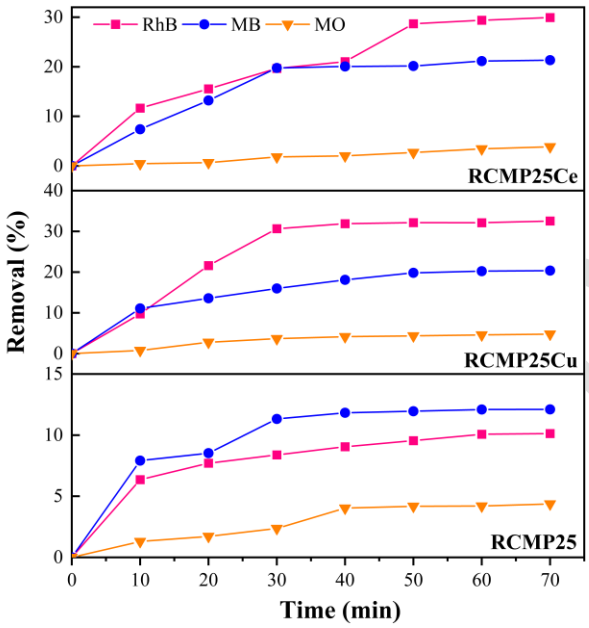

Fig. 6. Adsorption efficiency of three membranes with different organic dyes

The adsorption of the membranes can be further related to their porosity. The calculated porosity according (1) of RCMP25, RCMP25Cu, and RCMP25Ce were 76.47%, 84.64%, and 79.70%, respectively. The higher porosity of RCMP25Cu provides, a larger contact surface area and more open pore channels, facilitating dye diffusion into the membrane structure and increasing the number of available adsorption sites. This explains the significantly enhanced adsorption capacity of cationic dyes (MB and RhB) in RCMP25Cu compared to RCMP25 and RCMP25Ce. Conversely, the relatively lower porosity of RCMP25 results in fewer exposed pores and weaker adsorption capacity. Although RCMP25Ce has slightly lower porosity than RCMP25Cu, it still maintains a relatively porous structure, resulting in good adsorption capacity for MB and RhB. Adding powdered catalyst at an appropriate ratio can further enhance adsorption capacity, creating a more porous structure compared to the uncatalyzed membrane [7]. This behavior can be attributed to the chemical structure of cellulose, which is rich in negatively charged hydroxyl (–OH) groups, enabling strong electrostatic interactions with cationic dyes such as RhB and MB in aqueous solution. In contrast, MO possesses sulfonate ($–SO_3^-$) groups that render the negatively charged molecule in water, leading to electrostatic repulsion with the cellulose matrix. As a result, MO exhibits significantly lower adsorption on regenerated cellulose membranes compared to cationic dyes.

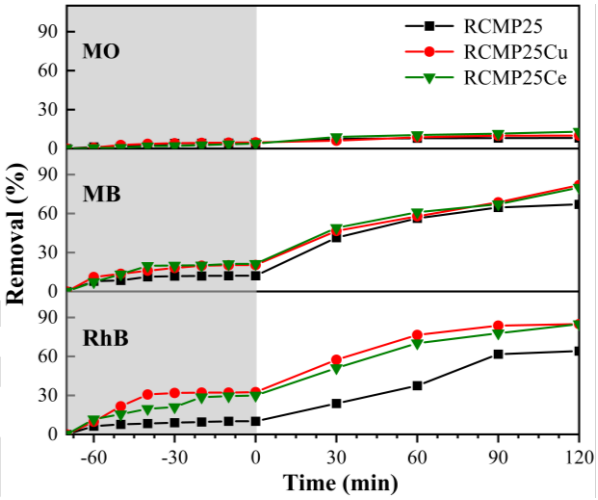

Fig. 7. Removal efficiency of MO, MB, and RhB by RCMP25, RCMP25Cu, and RCMP25Ce after adsorption in the dark (70 min) and subsequent photocatalytic degradation under Xenon lamp irradiation (120 min)

Fig. 8 presents the removal efficiencies of MO, MB, and RhB by RCMs after 70 min of adsorption in the dark and 120 min of Xenon lamp irradiation. For RhB, RCMP25Cu and RCMP25Ce achieved total removal efficiencies of 84.95% and 84.89%, respectively, which are significantly higher than that of RCMP25 (64.17%). This improvement can be due to the presence of copper and cerium species, which facilitate charge separation and increase the photocatalytic activity of materials. A similar result was seen in MB degradation, with RCMP25Cu and RCMP25Ce removing 81.91% and 79.91% of MB after 120 minutes of light, respectively, surpassing RCMP25 (67.13%). Our previous study also demonstrated that regenerated cellulose membranes without photocatalysts exhibit no additional dye removal under light irradiation, achieving only approximately 13.6% removal via adsorption in the dark [7, 8]. In contrast, MO showed a markedly lower RE, reaching only about 10% after 120 min of illumination. The lower degradation efficiency of MO

compared to MB and RhB is attributed to the electrostatic surface properties of the RC membrane. Zeta potential measurements ζ equal -20 mV confirm that the RC matrix is negatively charged due to abundant hydroxyl groups [15]. Consequently, the membrane preferentially adsorbs cationic dyes (MB, RhB) through electrostatic attraction-achieving up to 32.3% adsorption for RhB-while repelling anionic MO (adsorption approximately 4%). As surface adsorption is a critical precursor to photocatalysis, this electrostatic repulsion limits MO degradation to approximately 10%.

In general, the mechanism of ODs removal by RCMs involves two main processes: adsorption and photocatalytic degradation. First, the cellulose membrane contains hydroxyl groups that participate in the adsorption of cationic dyes (MB and RhB) through electrostatic attraction. Conversely, the anionic nature of MO causes electrostatic repulsion, hindering the adsorption process of the RC membranes. Then, under irradiation, pure P25 in the cellulose membrane generates reactive oxygen species (·OH, $\cdot O_2^-$) that degrade pollutants, but its efficiency is limited by a wide band gap and rapid electron-hole recombination. Doping Cu and Ce into P25 and immobilizing these catalysts on the cellulose membranes has overcome this limitation, contributing to improved efficiency in the removal of ODs [16].

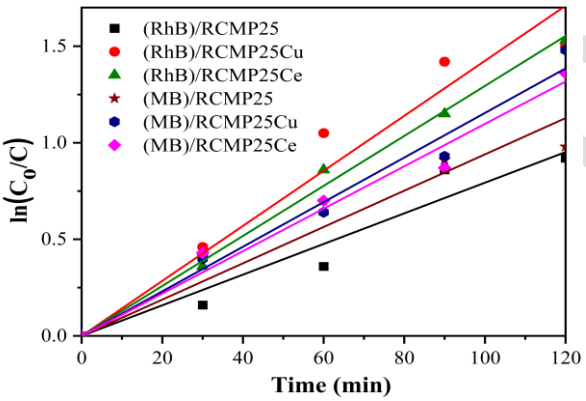

Fig. 8. Pseudo-first-order kinetic plots for the photocatalytic degradation of RhB and MB by RCMP25, RCMP25Cu, and RCMP25Ce under Xenon lamp illumination

Table 2. Kinetic parameters for organic dyes' degradation

Dyes		Units	RCM P25	RCM P25Cu	RCM P25Ce
MB	k_1	min^{-1}	0.009	0.012	0.011
	R^2		0.975	0.993	0.992
RhB	k'_1	min^{-1}	0.008	0.014	0.130
	R^2		0.976	0.982	0.998

As shown in Fig. 9 and Table 2, the photocatalytic degradation of both RhB and MB follows pseudo-first-order kinetics for three composite membranes. The rate constants of RCMP25Cu and RCMP25Ce are consistently higher than that of RCMP25, indicating that the incorporation of Cu- and Ce-modified photocatalysts effectively enhances the degradation kinetics. This improvement can be attributed to the presence of metal dopants, which promote charge separation and suppress electron–hole recombination, thereby increasing the generation of reactive species. In contrast, RCMP25 exhibits lower rate constants, such as k_1' equal 0.008 min^{-1} (RhB) and k_1 equal 0.009 min^{-1} (MB). These outcomes are consistent with the general degradation efficiencies discussed above, which helps support the advantageous impact of Cu and Ce on enhancing photocatalytic activity.

4. Conclusion

Regenerated cellulose membranes were successfully fabricated with different photocatalysts via a simple dissolution–coagulation method, forming stable composite membranes without changing the chemical bonding, phase structure, or thermal properties of either cellulose or the catalysts. The cellulose structure allows the uniform catalyst distribution and effective immobilization to remove contamination from water and recover catalyst powder after treatment. RCMP25Cu and RCMP25Ce exhibited significantly enhanced removal efficiencies toward cationic dyes, achieving up to 84.95% RhB and 81.91% MB removal under Xenon lamp irradiation, while showing limited efficiency toward anionic dyes. These results demonstrate that regenerated cellulose provides a versatile, sustainable platform for fixing different photocatalysts and highlight the potential of such composite membranes for environmentally friendly water treatment applications.

Acknowledgments

This research was supported by RoHan Project funded by the German Academic Exchange Service (DAAD, No. 57315854), and the Federal Ministry for Economic Cooperation and Development (BMZ) inside the framework "SDG Bilateral Graduate School Programme".

References

[1] H. Kolya and C.-W. Kang, Toxicity of Metal Oxides, Dyes, and Dissolved Organic Matter in Water: Implications for the Environment and Human Health, Toxics, vol. 12, p. 111, Jan. 2024. https://doi.org/10.3390/toxics12020111

[2] M. Berradi, R. Hsissou, M. Khudhair, M. Assouag, O. Cherkaoui, A. El Bachiri, and A. El Harfi, Textile finishing dyes and their impact on aquatic environs, Heliyon, vol. 5, iss. 11, Nov. 2019, Art. no. e02711. https://doi.org/10.1016/j.heliyon.2019.e02711

[3] M. Sarkar, A. Upadhyay, D. Pandey, C. Sarkar, and S. Saha, Cellulose-Based Biodegradable Polymers: Synthesis, Properties, and Their Applications, in Biodegradable Polymers and Their Emerging Applications, Singapore: Springer, 2023, pp. 89–114. https://doi.org/10.1007/978-981-99-3307-5_5

[4] Y. Deng, T. Zhu, Y. Cheng, K. Zhao, Z. Meng, J. Huang, W. Cai, and Y. Lai, Recent Advances in Functional Cellulose-Based Materials: Classification, Properties, and Applications, Adv. Fiber Material, vol. 6, pp. 1343–1368, Jun. 2024. https://doi.org/10.1007/s42765-024-00454-0

[5] M. Bissenova, N. Idrissov, Z. Kuspanov, A. Umirzakov, and C. Daulbayev, Hybrid adsorption–photocatalysis composites: A sustainable route for efficient water purification, Materials for Renewable and Sustainable Energy, vol. 14, pp. 44, Jul. 2025. https://doi.org/10.1007/s40243-025-00319-5

[6] D. Fabbri, M. J. López-Muñoz, A. Daniele, C. Medana, and P. Calza, Photocatalytic abatement of emerging pollutants in pure water and wastewater effluent by TiO_2 and Ce-ZnO: Degradation kinetics and assessment of transformation products, Photochemical & Photobiological Sciences, vol. 18, pp. 845–852, Oct. 2020. https://doi.org/10.1039/C8PP00311D

[7] V. Q. Nguyen, P. M. Cao, B. C. Nguyen, T. M. Le, and M. N. Nguyen, Enhancing photocatalytic performance by immobilizing varying TiO_2 contents on composite regenerated cellulose membrane: An environmentally reusable membrane, Research on Chemical Intermediates, vol. 51, pp. 5383–5408, Aug. 2025. https://doi.org/10.1007/s11164-025-05705-2

[8] M. N. Nguyen, T. M. Truong, V. Q. Nguyen, P. M. Cao, T. T. Thi, and B. C. Nguyen, Enhancing transparency and performance of regenerated cellulose membrane for organic dye treatment: the role of dimethyl sulfoxide in structural modification, Cellulose, vol. 32, pp. 4553–4572, May 2025. https://doi.org/10.1007/s10570-025-06496-w

[9] M. Abe, Y. Fukaya, and H. Ohno, Fast and facile dissolution of cellulose with tetrabutylphosphonium hydroxide containing 40 wt% water, Chemical Communications, vol. 48, pp. 1808–1810, Nov. 2012. http://dx.doi.org/10.1039/C2CC16203B

[10] Q. V. Nguyen, M. T. Truong, T. T. T. Do, and N. M. Nguyen, Organic dyes and perfluorooctanoic acid decompositions by cerium- and copper-modified commercial TiO_2 under visible light, Journal of Science and Technology: Engineering and Technology for Sustainable Development, vol. 36, iss. 1, pp. 028–035, Mar. 2026. https://doi.org/10.51316/jst.189.etsd.2026.36.2.4

[11] S. Y. Oh, D. I. Yoo, Y. Shin, H. C. Kim, H. Y. Kim, Y. S. Chung, W. H. Park, and J. H. Youk, Crystalline structure analysis of cellulose treated with sodium hydroxide and carbon dioxide by means of X-ray diffraction and FTIR spectroscopy, Carbohydrate Research, vol. 340, pp. 2376-2391, Oct. 2005. https://doi.org/10.1016/j.carres.2005.08.007

[12] M. N. Nguyen, M. T. L. Nguyen, M. Frank, and D. Hollmann, Beyond waste: cellulose-based biodegradable films from bio waste through a cradle-to-cradle approach, RSC Sustainability, vol. 2, pp. 4028–4035, Nov. 2024. https://doi.org/10.1039/d4su00613e

[13] Q. Wang, G. Chen, Z. Yu, X. Ouyang, J. Tian, and M. Yu, Photoluminescent Composites of Lanthanide-Based Nanocrystal-Functionalized Cellulose Fibers for Anticounterfeiting Applications, ACS Sustainable Chemistry & Engineering, vol. 6, pp. 13960-13967, Nov. 2018. https://doi.org/10.1021/acssuschemeng.8b02307

[14] E. Bêche, P. Charvin, D. Perarnau, S. Abanades, and G. Flamant, Ce 3d XPS investigation of cerium oxides and mixed cerium oxide ($Ce_xTi_yO_z$), Surface and Interface Analysis, vol. 40, pp. 264-267, Jan. 2008. https://doi.org/10.1002/sia.2686

[15] M. N. Nguyen, U. Kragl, I. Barke, R. Lange, H. Lund, M. Frank, A. Springer, V. Aladin, B. Corzilius, and D. Hollmann, Coagulation using organic carbonates opens up a sustainable route towards regenerated cellulose films, Communications Chemistry, vol. 3, pp. 116, Aug. 2020. https://doi.org/10.1038/s42004-020-00360-7

[16] M. Pawar, S. Topcu Sendoğdular, and P. Gouma, A Brief Overview of TiO_2 Photocatalyst for Organic Dye Remediation: Case Study of Reaction Mechanisms Involved in Ce-TiO_2 Photocatalysts System, Journal of Nanomaterials, vol. 2018, pp. 5953609, Jan. 2018. https://doi.org/10.1155/2018/5953609